CIENCIA 14 (Special Number on Adsorption and Catalysis), 83 - 95, 2006
Maracaibo, República Bolivariana de Venezuela

# Modeling interaction of pyridine on $Mo_2CuS_8$ for the HDN reaction. A theoretical study

*Aldo Munaretto[1], Fernando Ruette[2]*, Morella Sánchez[2] y Eloy Rodríguez-Arias[1]*

*[1]Laboratorio de Modelaje en Catálisis, Departamento de Química, Universidad Simón Bolívar, Apartado 89000, Caracas 1080-A, Venezuela. [2]Laboratorio de Química Computacional, Centro de Química, Instituto Venezolano de Investigaciones Científicas (IVIC), Apartado 21827, Caracas 1020-A, Venezuela*

Received: 28-11-05 Accepted: 12-01-06

## Abstract

The role of Cu in the hydrodenitrogenation (HDN) of pyridine on molybdenum sulfide surface is studied with a CNDO method reparameterized for diatomic binding energies. A model system of a hydrogenated $Mo_2MeS_8$ cluster (Me = Cu or Mo) and a pyridine molecule were used to simulate the HDN process. Theoretical results show that the highest adsorption energy is found on the copper atom when this metal is located in a central position between two Mo atoms. Furthermore, the best adsorption mode occurs to the case in which the pyridine $C_{2v}$ axis is parallel to the Cu-S-Mo axis. Pyridine hydrogenation is explained by a notable interaction between hydrogen atoms adsorbed on Mo atoms neighboring the adsorption site and C and N atoms of the organic compound. Copper adsorption site presents: (a) A negative charge density due to electronic transference from lateral Mo atoms. (b) Weaker Me-S and Me-Mo bonds than in the case of pure $MoS_2$, which makes difficult to substitute Mo by Cu. (c) The Mo-S bonds are stronger in $Mo_2CuS_8$ than in $Mo_3S_8$, which does not facilitate adjacent vacancy formation around the adsorption site and impedes the pyridine hydrogenation.

**Key words:** CNDO; HDN; $MoS_2$; $Mo_2CuS_8$; pyridine hydrogenation; theoretical.

# Modelaje de la reacción de HDN por medio de la interacción de piridina sobre $Mo_2CuS_8$. Un estudio teórico

## Resumen

El papel del Cu en la hydrodesnitrogenación (HDN) de la piridina sobre una superficie de sulfuro de molibdeno es estudiado con el método CNDO, reparametrizado para el cálculo de las energías diatómicas de enlace. Para simular el proceso de HDN se utilizó como sistema modelo un agregado hidrogenado de $Mo_2MeS_8$ (Me= Cu o Mo) y una molécula de piridina. Los resultados teóricos muestran que la mayor energía de adsorción se encuentra cuando el átomo de Cu se localiza en una posición central entre dos átomos de Mo. Además se encontró que el mejor modo de adsorción ocurre cuando el eje $C_{2v}$ de la piridina es paralelo al eje Cu-S-Mo. La hidrogenación de la piridina se explica por la fuerte interacción que ocurre entre los átomos de hidrógeno ad-

* Autor para la correspondencia. E-mail: fruette@ivic.ve

sorbidos sobre los átomos de Mo vecinos al sitio de adsorción y los átomos de C y N del compuesto orgánico. Cuando la adsorción ocurre sobre el Cu se observa: a) Una carga negativa sobre el Cu debida a la transferencia electrónica de los átomos de Mo laterales. b) Los enlaces Me-S y Me-Mo son más débiles que en el caso del $MoS_2$ puro, lo cual explica la dificultad de sustitución de Mo por Cu. c) Los enlaces Mo-S en $Mo_2CuS_8$ son más fuertes que en $Mo_3S_8$, lo cual desfavorece la formación de vacancias alrededor del sitio de adsorción e impide la hidrogenación de la piridina.

**Palabras clave:** Cálculos teóricos; CNDO; hidrogenación de piridina; HDN; $MoS_2$; $Mo_2CuS_8$.

## 1. Introduction

Nowadays it is necessary more effective catalysts for oil processing due to the increasing use of low quality oil (heavy oil and heavier fractions from refineries) and ecological requirements. Clean fractions of oil avoid environmental pollution by elimination of sulfur and nitrogen compounds and prevent refinery catalysts poisoning by metal deposition. To solve this problem entails the removal of sulfur (hydrodesulfurization (HDS)), nitrogen (HDN), oxygen (hydrodeoxygenation (HDO)), and heavy metals (hydrodemetallation (HDM)), from crude oil (1) by hydrotreatment.

Transition metals sulfides on support materials, with a high surface area, are broadly used in hydrotreatment and upgrading processes of standard oil, due to their catalytic and structural stability to transform feedstocks with large amounts of sulfur and other contaminants (2).

It is widely recognized that hydrogenation is a step of primary importance (3, 4) in HDN, because the saturated molecule is that that loses nitrogen. However, Cattenot et al. (5) found that the reaction mechanism depends on the substrate structure to be transformed and on the transition metal sulfide catalyst properties. So, it can proceeds via elimination or by a nucleophilic substitution. Two different types of sites may be involved; i.e., vacancies and acid-basis sites.

The sulfides of Ru, Os, Ir, and Rh are the most actives in hydrotreatment processes (1, 6), but they are also too expensive. Generally, metal sulfides of VIb group are combined with promoting metals of the VIII group, in order to modify the electronic configuration of the catalyst (7, 2). CoMoS and NiMoS phases supported on alumina are largely employed in hydrotreatment processes, where the vacancy sites are determining factors in the reaction rate.

Molybdenum sulfide appears as an important catalyst for amines conversion (4). On the other hand, there is a correlation between HDN activity for an industrial charge and the number of Mo atoms at corners and edges of $MoS_2$ crystallites (3). Thus, catalytic properties are dominated by the crystal structure anisotropy. Active sites are sulfide vacancies located at edges and corners of the $MoS_2$ catalyst (7). There is a general agreement that the most active sites are in the M-M'-S phase (M = metal of group VIII and M' = metal of group VIb). Luchsinger et al. (8) found that bringing mixed metals (Ni/Mo sulfide) in intimate contact by sulfur bonds creates more active catalysts for the HDN of quinoline.

The role of copper as promoter is, however, not clear. Harris and Chianelli (9) found that Cu and Cr inhibit the catalytic activity of the $MoS_2$ catalysts. These metals withdraw electronic density from Mo and reinforce the Mo-S bonds, hindering the vacancy formation. Otherwise, Lindner et al. (10) with only a little quantity of copper in $MoS_2$ obtained a great activity in the HDS reaction of thiophene.

The purpose of this paper is to clarify the role of the copper as promoter in the HDN reaction. In this work, a pyridine molecule, used as a nitrogen compound model, is studied in different bonding adsorption modes and on different sites of a $MoS_2$ surface model doped with copper, used as catalyst. The catalytic surface is represented by a $Cu/Mo_2S_8$ model cluster and by a partially hydrogenated $Cu/Mo_2S_8H_2$ one.

In the following Section, pyridine HDN reactions and the model surface employed here are discussed. In Section 3, a brief description of the method used for calculation of binding energies and parameters is presented. Pyridine adsorptions on the different surface sites without and with hydrogen are analyzed in Sections 4 and 5. Finally, in Section 6, some remarkable results are presented as conclusions.

## 2. Pyridine reaction and surface model

Several schemes have been propose for pyridine HDN process according to the nature of active site, vacancy formation, and reaction mechanism. Ledoux et al. (11) found that ruthenium sulfide was six times more active than $MoS_2$ for pyridine conversion. On the other hand, McIlvried (12) proposed that the determining step in the HDN reaction is the hydrogenolysis of pyperidine to n-penthylamine in a $NiMo/Al_2O_3$ catalyst. This is confirmed by Satterfield et al. (13), who showed that hydrogenation reaction takes place before hydrogenolysis. Rodríguez et al. (14) compared the HDN reaction between the pyridine and the ciclohexylamine on pure and Ni-promoted MoSx films and S/Mo(110) surfaces. They found that pyridine was weakly chemisorbed and most of them desorbed at temperatures around 200 K, while Mo centers with a limited number of S vacancies are able to cleave the C-N bond.

In general, it is accepted that the mechanism for the HDN reaction in pyridine proceeds via hydrogenation of the aromatic ring, followed by hydrogenolysis of the C-N bond:

$$C_5H_5N + 3H_2 \leftrightarrow C_5H_{10}NH \xrightarrow{H_2\ slow} C_5H_{11}NH_2 \xrightarrow{H_2} C_5H_{12} + NH_3$$

Hydrogenation of the heteroring is required to reduce the relatively large energy of aromatic C-N bonds, in order to facilitate their scissions.

The surface model used for studying the HDN reaction between the pyridine and $Cu/MoS_2$ was similar to that employed previously (15). A single slab structure ($Mo_3S_8$) with Mo sites completely exposed (vacancies) was chosen, because experimentally it is known that the catalytic surface is pretreated with $H_2$. This tiny slab corresponds to the corner of small $MoS_2$ crystal that has been reported as the place in which active sites are located (3). The total cluster charge is zero. The $Cu/MoS_2$ model is obtained when in $Mo_3S_8$ one of the Mo atoms is substituted by Cu in two different places: in the edge or in the center of the model, as shown in Figure 1. The adsorption of the pyridine is studied in both sites on Mo and on Cu.

Calculations with different spin multiplicities and full optimization were performed for the models 1(a) and 1(b). The optimal spin multiplicities were 4 and 6, respectively. The calculated Cu-Mo (2.80 Å, for center Cu and 2.87 Å for edge Cu) and Cu-S distances (2.20 and 2.23 Å, respectively) are similar to the DFT values of Raybaud et al. (16). For the pyridine molecule, the geometric values by Del Bene (17) were used.

## 3. Computational details

Calculations were performed by using the CNDO-UHF method from GEOMO program (18) with several modifications (19), such as, the calculation of diatomic binding energies and Mulliken population with orthogonal molecular orbitals (20).

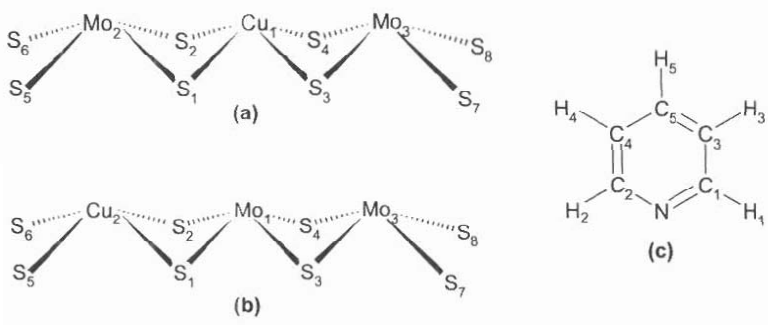


Figure 1. Structure of $CuMo_2S_8$: (a) with Cu in the center; (b) with Cu on the edge; (c) Pyridine

Since CNDO overestimates binding energies (21), a parameterization, used in other works, was done per each bond, in order to calculate reasonable total binding energies (*TBE*) (22). *TBE* is calculated in terms of parameterized diatomic binding energies (*PDBE*) (23) obtained from calculated diatomic binding energies (*DBE*) as follows:

$$DBE_{(AB)} = \varepsilon_{AB} + f_B(AB)\Delta\varepsilon_A + f_A(AB)\Delta\varepsilon_B \quad [1]$$

where

$$f_A(AB) = \frac{\varepsilon_{AB}}{\sum_{C \neq AS} \varepsilon_{AC}} \quad [2]$$

and $\varepsilon_{AB}$ and $\Delta\varepsilon_A$ are diatomic and monoatomic energy terms for *AB* bond and *A* atom, respectively.

Thus, *TBE* is evaluated as:

$$TBE = \sum_{A>B} PDBE(AB) \quad [3]$$

where

$$PDBE(AB) = \alpha_{AB} \cdot DBE(AB) \quad [4]$$

Here, $\alpha_{AB}$ is the ratio between the accurate (experimental or theoretical) bond dissociation energy of a *A-B* diatomic molecule *DBE*(*A-B*) and the calculated (*CDBE*(*A-B*)); i.e.,

$$\alpha_{AB} = DBE(A-B)/CDBE(A-B) \quad [5]$$

The Cu parameters were calculated by varying the core integral in order to reproduce ionization potentials of the Cu atom. Slater exponents (24) were adjusted to obtain the electronic configuration of the atom ($[Ar]3d^{10}4s^1$), and $\beta$ values were calculated in such a way to reproduce the interatomic distance in Cu-N molecule (25). These values were tested calculating the geometry from different molecules with Cu-H, Cu-N, Cu-S and Cu-C bonds (26). The intermolecular distance and the *DBE*(Cu-Mo) were calculated using Gaussian 98, B3LYP, with the LanL2DZ base for Cu and the Yanagisawa et al. atomic base for Mo (26h). The $\alpha_{AB}$ were obtained for N-H, N-C, N-S, N-Mo, Cu-H, Cu-C, Cu-N, Cu-S, and Cu-Mo. Other $\alpha_{AB}$ bond parameters are reported in previous work (23). The calculated set of parameters is shown in Table 1.

To analyze the pyridine-catalyst interaction, the adsorption energy was calculated as the difference between the *TBE* of the catalyst with pyridine adsorbed and the sum of *TBE*s of isolated pyridine and catalyst; i.e.

$$E_{adsorption} = TBE_{system + pyridine} - (TBE_{system} + TB_{Epyridine}) \quad [6]$$

## 4. Pyridine Adsorption

Pyridine can be adsorbed with different bonding modes and on different sites of the surface. Adsorption on the two metals were performed by considering different orienta-

Table 1
Parameters for Cu atom and $\alpha$ values for *A-B* bonds.

| Atomic Parameters | | Diatomic Parameters | |
|---|---|---|---|
| Orbital | Slater exponent | Bond (*A-B*) | $\alpha_{AB}$ |
| 4s | 1.50 | N-H | 0.4252 |
| 4p | 1.21 | N-C | 0.3281 |
| 3d | 1.70 | N-S | 0.9050 |
| | Core Integral (eV) | N-Mo | 0.6027 |
| 4s | 3.62 | Cu-H | 0.2225 |
| 4p | 1.00 | Cu-C | 0.1352 |
| 3d | 3.66 | Cu-N | 0.0578 |
| | $\beta$ (eV) | Cu-S | 0.1135 |
| 4s | 20.00 | Cu-Mo | 0.0914 |
| 4p | 20.00 | - | - |
| 3d | 26.00 | - | - |

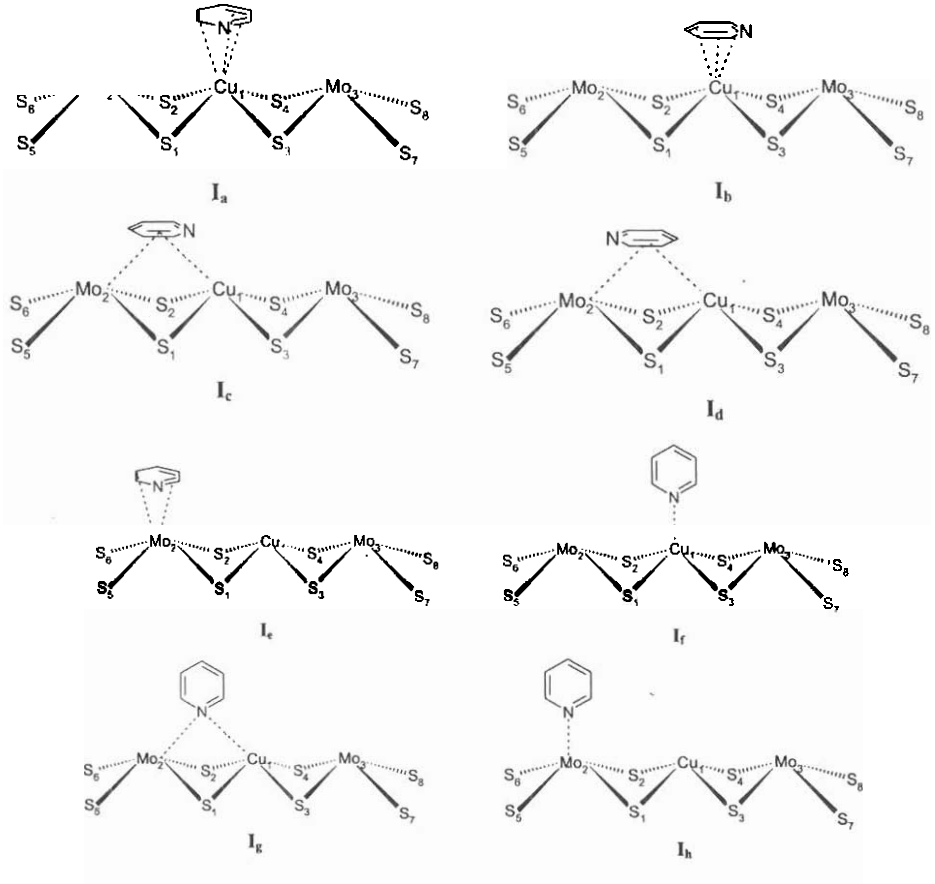


Figure 2. Pyridine adsorption modes on $CuMo_2S_8$ with Cu atom in the center

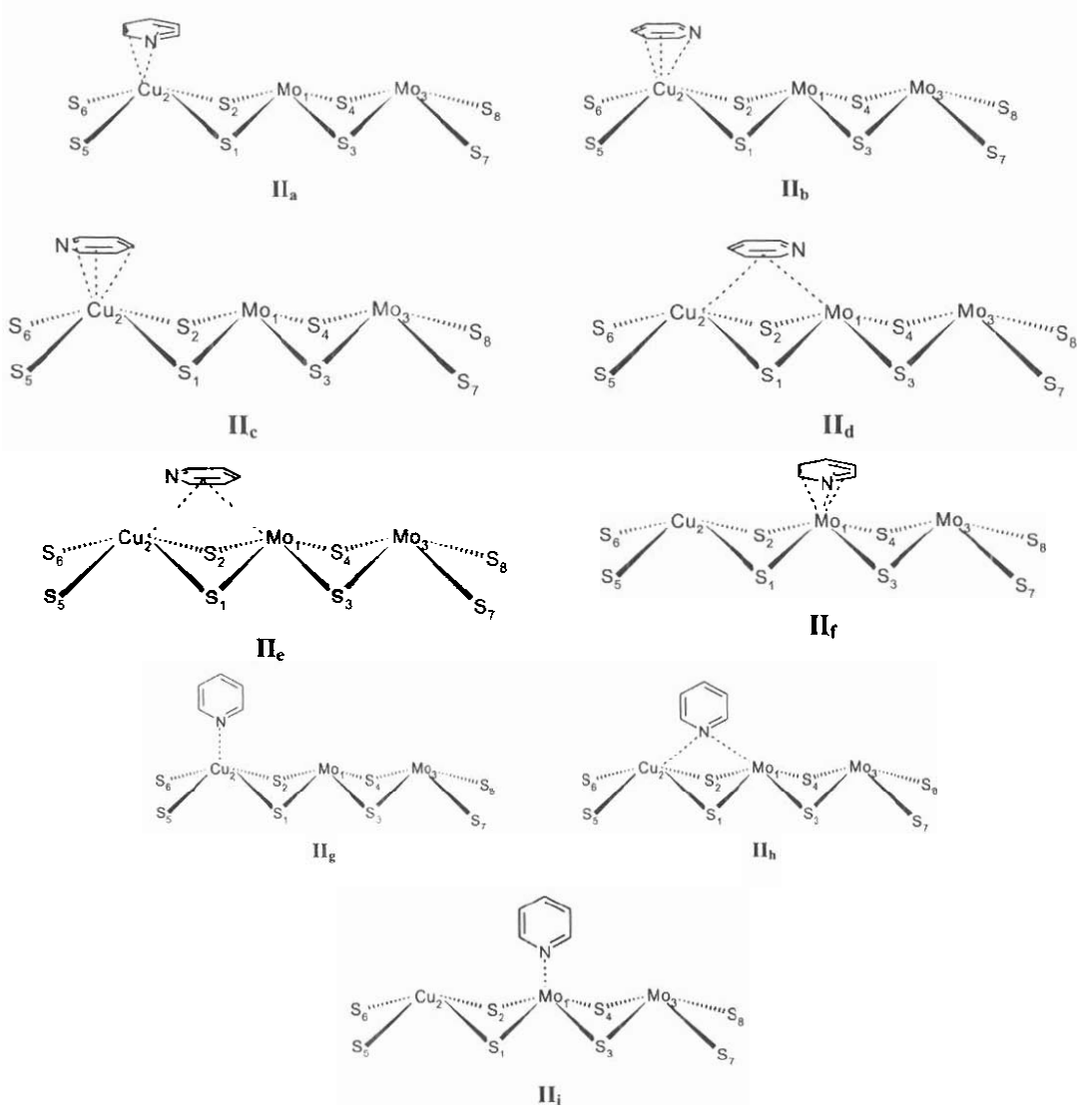


Figure 3. Pyridine adsorption modes on $CuMo_2S_8$ with Cu atom in the edge.

tions of the pyridine ring plane with respect to the surface plane, i.e., parallel ($\pi$-coordinate mode) and perpendicular ($\sigma$-coordinate mode). These diverse adsorption modes are shown in Figure 2 and 3, where the system has a central or an edge Cu atom, respectively. Potential energy curves, for determining the optimal adsorption distances, were made in each case. The corresponding total energy values for these distances are displayed in Table 2.

The system with the highest stability in total energy is depicted in $I_a$, followed by the structures depicted in $I_b$, $II_c$, $I_d$, and $II_b$, see adsorption modes in Figures 2 and 3. Note that the most stable systems are those that exhibit a $\pi$-adsorption mode of pyridine on the Cu atom, followed by those with a $\pi$-adsorption in a site between Mo and Cu atoms; and finally, the smallest adsorption energies correspond to the $\sigma$-adsorption mode as well as on a Cu or Mo atom. Note

Table 2
Total energies at the optimal interaction distances for I and II systems shown in Figures 2 and 3, respectively.

| System | Optimal interaction distances (Å) | Total energies (a.u.) |
|---|---|---|
| $I_a$ | 1.80 | -189.377164 |
| $I_b$ | 1.85 | -189.312584 |
| $I_c$ | 2.06 | -189.118223 |
| $I_d$ | 2.08 | -189.159229 |
| $I_e$ | 1.82 | -189.066268 |
| $I_f$ | 2.02 | -188.738547 |
| $I_g$ | 1.75 | -188.795702 |
| $I_h$ | 1.93 | -188.678888 |
| $II_a$ | 1.78 | -189.099563 |
| **$II_b$** | **1.77** | **-189.138945** |
| $II_c$ | 1.83 | -189.161498 |
| $II_d$ | 2.07 | -188.970917 |
| $II_e$ | 2.06 | -188.918655 |
| $II_f$ | 1.92 | -188.979889 |
| $II_g$ | 2.01 | -188.509123 |
| $II_h$ | 1.73 | -188.610464 |
| $II_i$ | 1.93 | -188.488058 |

Table 3
Adsorption energies for the most stable systems.

| System | Adsorption energy (kcal/mol) |
|---|---|
| $I_a$ | -95.818 |
| $I_c$ | -69.641 |
| $II_a$ | -62.902 |
| $II_c$ | -60.106 |
| $II_f$ | -85.758 |

that the energy difference between the first and the fifth most stable systems is of 0.24 au (about 149 kcal/mol). This unrealistic big difference is solved by calculating the parameterized adsorption energy for the most stable systems, using Eqs. [3] and [6] (Table 3). Results show that the adsorption in the $I_a$ system is again the most favorable and the $\pi$-adsorption is still preferred that the $\sigma$-adsorption mode, but the order in energy is changed.

We found that the systems with the highest adsorption energy ($I_a$, $II_f$), are those that present the $C_{2v}$ pyridine axis perpendicular to the Mo-Cu-Mo axis, and the adsorption is on the central atom (Cu for $I_a$ and Mo for $II_f$ systems).

A detailed understanding of the adsorbate activation is performed by analyzing the PDBEs of the adsorbed and the isolated pyridine, as it is presented in the Table 4 for the most stable systems. Here, it can be observed that the largest activation occurs in the $I_a$ system. The major N-C bond activation occurs mainly when the pyridine is adsorbed on a Cu atom (central, $I_a$, or edge, $II_a$). On the other hand, the smallest activation on the N-C bond is found for the $I_c$ and $II_f$ adsorption modes, with the pyridine adsorbed on a Mo atom. Notice that C-H and C-C bonds are weakened, facilitating the formation of other C-H bonds, as it will show below.

## 5. Adsorption on a partially hydrogenated surface

Due to the fact that the most activated pyridine is obtained when the adsorption occurs in the $I_a$ mode, the surface model with the central Cu atom is used to study the hydrogenated $CuMo_2H_2S_8$ system, as shown in Figure 4. The optimal spin multiplicity found for this model surface was 6 for different adsorption modes depicted in Figure 5. It is also found that the $\pi$-adsorption mode is preferred (system $III_b$ and $III_a$) over the $\sigma$ one (system $III_c$), as can be seen in Table 5,

Table 4
Pyridine bonding properties (*PDBE* (kcal/mol)) of the most stable systems

| System Bond | $I_a$ | $I_c$ | $II_a$ | $II_c$ | $II_f$ | Isolated pyridine |
|---|---|---|---|---|---|---|
| N-$C_1$ | -111.0 | -119.3 | -110.6 | -114.9 | -119.4 | -131.2 |
| N-$C_2$ | -111.0 | -118.2 | -117.8 | -114.9 | -120.5 | -131.2 |
| $C_1$-$C_3$ | -102.9 | -99.4 | -101.8 | -110.3 | -103.8 | -117.9 |
| $C_2$-$C_4$ | -102.9 | -106.5 | -108.1 | -110.3 | -102.2 | -117.9 |
| $C_3$-$C_5$ | -103.0 | -107.0 | -103.8 | -100.8 | -107.9 | -117.4 |
| $C_4$-$C_5$ | -103.0 | -107.2 | -104.1 | -100.8 | -108.4 | -117.4 |
| $C_1$-$H_1$ | -87.7 | -91.7 | -86.5 | -98.3 | -91.0 | -103.5 |
| $C_2$-$H_2$ | -87.7 | -97.8 | -96.8 | -98.3 | -94.0 | -103.5 |
| $C_3$-$H_3$ | -87.7 | -91.4 | -87.4 | -97.7 | -91.6 | -103.1 |
| $C_4$-$H_4$ | -87.7 | -98.7 | -98.8 | -97.7 | -94.1 | -103.1 |
| $C_5$-$H_5$ | -98.4 | -97.9 | -97.4 | -80.5 | -98.2 | -102.3 |

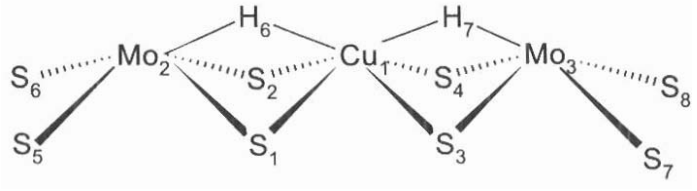


Figure 4. Model $CuMo_2H_2S_8$ cluster.

where total energies at the optimal interaction distances are displayed.

The most stable system is when the pyridine $C_{2v}$ axis is parallel to the Mo-Cu-Mo axis of the surface. To a better understanding of pyridine adsorption, the bonding properties of the most stable system ($III_b$) are presented in Table 6. In this Table are also presented the bonding properties of the analogous $Mo_3H_2S_8$-pyridine system in order to elucidate the role of copper in the HDN of pyridine.

Results show that Cu-N and Cu-H bonds are weaker than those of Mo-N and Mo-H. The interaction between the central metal atom (Cu or Mo) and the pyridine C atoms are not so different. Additionally, there is not a big disparity when Cu or Mo is present for the interaction between the terminal Mo atoms ($Mo_2$ and $Mo_3$) with carbon, nitrogen and hydrogen atoms of pyridine. However, interactions of superficial H atoms ($H_6$, $H_7$, Figure 5) with the pyridine show notable differences. *PDBE* values of the $H_6$-$C_5$ bond vary from -14.4 kcal/mol, in the $Mo_3H_2S_8$ model, to -47.5 kcal/mol in the surface with copper, and similarly $H_7$-N bond goes from -9.7 to -42.2 kcal/mol, respectively. These important bonds with the adsorbed superficial H atoms consequently produce a fair weakening of N-$C_1$ and $C_3$-$C_5$ pyridine bonds from -131.2 to -106.8 and from -117.9 to -96.7 kcal/mol in $CuMo_2H_2S_8$-$C_5H_5N$, respectively.

The pyridine adsorption has not a significant effect on the Mo-Cu bond, contrary to the Mo-Mo in which a change from -55.1 to -30.1 kcal/mol occurs. Another important issue is the lability of the superficial Hs

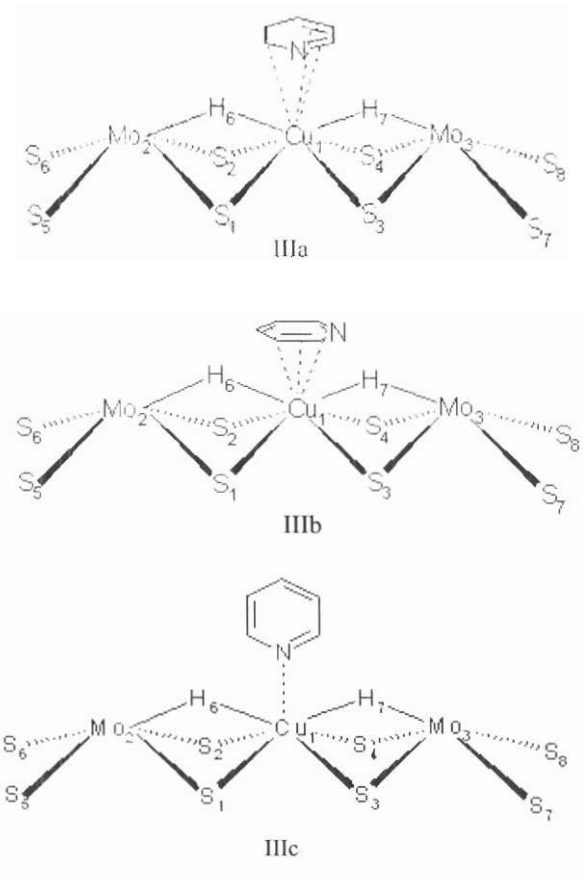


Figure 5. Hydrogenated systems: (a) $\pi$-coordination, $C_{2v}$ pyridine axis perpendicular to Mo-Cu-Mo axis. (b) $\pi$-coordination, $C_{2v}$ pyridine axis parallel to Mo-Cu-Mo axis. (c) $\sigma$-coordination.

Table 5
Total energies at the optimal adsorption distances for the hydrogenated III systems, shown in Figure 5.

| System | Optimal interaction distance (Å) | Total energy (a.u.) |
|---|---|---|
| $III_a$ | 2.17 | -190.410 |
| $III_b$ | 2.26 | -190.421 |
| $III_c$ | 2.24 | -190.160 |

($H_6$, $H_7$). These Hs are bonded as well as to the central atom and to the lateral Mo atoms. The interaction of superficial H in the system without pyridine and with Cu (-33.7 kcal/mol) is weaker than that with Mo (-44.7 kcal/mol). The interaction of pyridine with $Mo_3H_2S_8$ reveals that the superficial Mo-H bonds do not vary significantly. On the other hand, in $CuMo_2H_2S_8$, the pyridine adsorption changes the Cu-$H_6$ bond from -33.7 to -11.8 and the $Mo_2$-$H_6$ from -64.1 to -19.8 kcal/mol. It means that the Cu doping on the catalyst increases the surface hydrogenation capability. Thus, the first hydrogenation step occurs via superficial hydrogen donation to N and $C_5$ pyridine atoms in the $III_b$ mode of adsorption.

Table 6
Comparison between the bonding properties (*PDBE*, kcal/mol) for $CuMo_2H_2S_8$-$C_5H_5N$ ($III_b$) and $Mo_3H_2S_8$-$C_5H_5N$ systems. Values in parentheses correspond to isolated systems ($CuMo_2H_2S_8$, $Mo_3H_2S_8$ and Pyridine). Me = central atom (Cu or Mo).

| Bond | $CuMo_2H_2S_8$-$C_5H_5N$ | $MoMo_2H_2S_8$-$C_5H_5N$ |
|---|---|---|
| Me-N | -1.9 | -13.7 |
| Me-$C_1$, $C_2$ | -13.4 | -13.2 |
| Me-$C_3$, $C_4$ | -14.2 | -12.8 |
| Me-$C_5$ | -10.0 | -11.2 |
| Me-$H_1$, $H_2$ | -1.1 | -4.9 |
| Me-$H_3$, $H_4$ | -0.9 | -5.3 |
| Me-$H_5$ | -0.4 | -5.1 |
| $Mo_2$-N | 3.6 | 2.0 |
| $Mo_2$-$C_3$, $C_4$ | -2.0 | -1.8 |
| $Mo_2$-$C_5$ | -10.2 | -10.4 |
| $Mo_2$-$H_3$, $H_4$ | -3.9 | -2.8 |
| $Mo_2$-$H_5$ | -24.6 | -28.4 |
| $Mo_3$-N | -20.9 | -24.9 |
| $Mo_3$-$C_1$, $C_2$ | -2.6 | -2.5 |
| $Mo_3$-$H_1$, $H_2$ | -4.0 | -2.8 |
| $H_6$-N | -0.3 | -0.4 |
| $H_6$-$C_5$ | -47.5 | -14.4 |
| $H_7$-N | -42.2 | -9.7 |
| *Pyridine* | – | – |
| N-$C_1$, $C_2$ | -106.8 (-131.2) | -118.2 |
| $C_1$-$C_3$, $C_2$-$C_4$ | -121.8 (-117.9) | -111.8 |
| $C_3$-$C_5$, $C_4$-$C_5$ | -96.7 (-117.4) | -106.4 |
| $C_1$-$H_1$, $C_2$-$H_2$ | -99.5 (-103.5) | -98.7 |
| $C_3$-$H_3$, $C_4$-$H_4$ | -100.4 (-103.1) | -100.2 |
| $C_5$-$H_5$ | -88.0 (-102.3) | -87.6 |
| *Cluster* | – | – |
| Me-$Mo_2$ | -22.1 (-23.6) | -30.1 (-55.1) |
| Me-$Mo_3$ | -22.0 (-23.6) | -33.2 (-55.1) |
| Me-$H_6$ | -11.8 (-33.7) | -43.1 (-44.7) |
| Me-$H_7$ | -12.7 (-33.7) | -41.4 (-44.7) |
| $Mo_2$-$H_6$ | -19.8 (-64.1) | -36.1 (-53.8) |
| $Mo_3$-$H_7$ | -25.8 (-64.1) | -34.3 (-53.8) |

The differences between pure $MoS_2$ and doped surfaces with Cu can be also explained by electronic charges on metallic atoms and pyridine, as shown in Table 7. Copper atom is negative charged (-0.20 and -0.31 au) as compared with Mo (0.68 au) and Mo edge atoms are more positively charged in doped surface than $MoS_2$. This suggests a donation of electronic density from $Mo_2$ and $Mo_3$ atoms to Cu, as has been reported by Harris and Chianelli (9). In addition, the pyridine molecule transfers more electronic charge to the surface when it is doped with Cu, see charge values for pyridine with adsorption modes $III_a$, $III_b$, and $III_c$ in Table 7. In all the cases, there is electronic charge transfer from the pyridine to the surface. This transference is higher to Cu than to Mo that may be considered as the cause of a major activation of pyridine when it is adsorbed on Cu.

The analysis of surface *DBE*s between metal and sulfur atoms can help to understand key processes in vacancy formation. Values of Mo-S and Cu-S are displayed in Table 8. It may observe that when Cu is added, the Mo-S bonds adjacent to the adsorption site become stronger. So, the required vacancies for the hydrotreatment process are more difficult to produce. That may leads to an inhibition in the HDN process as reported by Harris and Chianelli (9), due to inconveniences in the vacancy formation. On other hand, the Cu-S bond is weaker than the correspondent Mo-S. This indicates that replacement of Mo by Cu on the $MoS_2$ surface is difficult at local level. Thus, the observed promoter or inhibitor effects depend on the preparation of the catalyst, as suggested by Linder *et al.* (10).

## 6. Conclusions

A qualitative quantum mechanic method (reparameterized CNDO) and very simple models of surface ($Mo_2MeS_8$ (Me = Mo, Cu)) and reactant (pyridine) were used to interpret changes in the HDN process with

Table 7
Charges (au) on surface metal atoms in $III_b$ model and pyridine for the different models. Me = central atom (Cu or Mo).

| Atom/Pyridine | $Mo_3S_8$ | $Mo_3S_8H_2$-$C_5H_5N$ | $CuMo_2S_8$ | $CuMo_2S_8H_2$-$C_5H_5N$ |
|---|---|---|---|---|
| Me | 0.68 | 0.68 | -0.20 | -0.31 |
| $Mo_2$, $Mo_3$ | 0.75 | 0.74 | 0.97 | 1.04 |
| Pyridine in ($III_a$) | – | 0.16 | – | 0.45 |
| Pyridine in ($III_b$) | – | 0.16 | – | 0.38 |
| Pyridine in ($III_c$) | – | 0.25 | – | 0.36 |

Table 8
Bond properties (PDBE (kcal/mol) for metal-S atoms Me = central atom (Cu or Mo).

| Bond | $Mo_3S_8$ | $CuMo_2S_8$ |
|---|---|---|
| $Mo_2$-$S_6$,$S_7$ | -50.3 | -52.5 |
| $Mo_2$-$S_1$,$S_2$ | -44.5 | -53.2 |
| Me-$S_1$,$S_2$,$S_3$,$S_4$ | -43.6 | -32.7 |

Cu-doped $MoS_2$ catalyst. The catalytic activity is evaluated in terms of *DBE*s as a function of surface composition, location of the adsorption site (center or edge), and adsorption modes ($\pi$ or $\sigma$). The main highlights of this work are resumed as follows:

(a) Results show that the pyridine prefers to be absorbed on the copper central atom, mainly in a $\pi$-coordination mode.

(b) Copper atom site produces the major activation of pyridine bonds, therefore, it is expected that the Cu atom acts as an active site for the HDN, instead of promoting the activity of contiguous Mo atoms. It is observed an electronic charge transfer from neighboring Mo atoms to the Cu atom.

(c) The first step in the HDN process must to be the pyridine $\pi$-adsorption followed by the hydrogenation of N and $C_5$ atoms by adsorbed superficial H atoms in the reduced surface. Cu-doped $MoS_2$ catalyst has a higher capability to transfer H from the surface to the pyridine molecule than pure $MoS_2$ one.

(d) Copper increases the Mo-S *DBE*s of adjacent atoms around the adsorption site and consequently it must inhibit the vacancy formation, necessary to the HDN process.

(e) $MoS_2$ surfaces with Cu edge atoms are less actives that those with Cu inside the surface (central Cu atom). However, formation of Cu-S bonds at the center site is not favored with respect to the correspondent Mo-S ones. Thus, the preparation and synthesis is a determining factor in the activity of Cu-doped $MoS_2$ catalyst for HDN processes.

## Acknowledgment

This research has also been sponsored by FONACIT, Venezuela, with the G-9700667 and S1-2673 contracts.

## References

1. ANGELICI R.J. ***Polyhedron*** 16: 3073-3088, 1997.
2. CHIANELLI R.R. ***Sol St Chem in Catal*** Am. Chem. Soc., (SSCC) 221-234, 1985.
3. EIJBOUTS S., DE BEER V.H.J., PRINS R. ***J Catal*** 109: 217-220, 1988.
4. DELMON B. ***Bull Soc Chim Belg*** 104: 173-187, 1995.
5. CATTENOT M., PORTEFAIX J.L., AFONSO J., BREYSSE M., LACROIX M., PEROT G. ***J Catal*** 173: 366-373, 1998.
6. PECORATO T.A., CHIANELLI R.R. ***J Catal*** 67: 430-445, 1981.
7. RATNASARNY P., SIVASANKER S. ***Catal Rev Sc Eng*** 22: 401-429, 1980.
8. LUCHSINGER M.M., BOZKURT B., AK-GERMAN A., JANZEN C.P., ADDIEGO W.P., DARENSBOURG M.Y. ***Appl Cat*** 68: 229-247, 1991.
9. HARRIS S., CHIANELLI RR. ***J Catal*** 98: 17-31, 1986.
10. LINDNER J., VILLA GARCIA M.A., SACHDEV A., SCHWANK J. ***J Chem Soc Chem Comm*** 15: 1833-1835, 1989.
11. LEDOUX M., DJELLOULI B. ***J Catal*** 115: 580-590, 1989.
12. McILVRIED H.G. ***Ind Eng Chem Proc Res Dev*** 10: 125-130, 1971.
13. a) SATTERFIELD C.N., MODELL M., MAYER J.F. ***AlchE J*** 21: 1100-1107, 1975. b) SATTERFIELD C.N., COCHETTO J.F. ***AlchE J*** 21:1107-1111, 1975.
14. RODRIGUEZ J.A., DVORAK J., JIRSAK T., LI S.Y., HRBEK J. ***J Phys Chem B*** 103: 8310-8318, 1999.
15. GAINZA A.E., RODRÍGUEZ ARIAS E.N., RUETTE F. ***J Mol Catal*** 85: 345-359,1993.
16. RAYBAUD P., HAFNER J., KRESSE G., KASZTELAN S., TOULHOAT H. ***J Catal*** 190: 128-143, 2000.
17. DEL BENE J. ***J Am Chem Soc*** 101: 7146-7151, 1979.

18. RINALDI D. ***"GEOMO Program"***, QCPE, N€290, 1976.

19. a) HERNANDEZ A.J., RUETTE F., LUDEÑA E.V. ***J Mol Catal*** 39: 21-41, 1987.
b)RUETE F., ESTIU G., JUBERT A.J., PISDIEZ R. ***Rev Ven Soc Catal*** 13: 57-64, 1999.

20. a) FISHER H., KOLLMAR H. ***Theor Chim Acta*** 16: 163-174, 1970.
b) SANCHEZ M., RUETTE F. ***J Mol Struct (Theochem)*** 254: 335-342, 1992.
c) SIERRAALTA A., FRENKING G. ***Theor Chim Acta*** 95: 1-12, 1997.

21. RODRIGUEZ ARIAS E.N., GAINZA A.E., HERNANDEZ A.J., LOBOS P.S., RUETTE F. ***J Mol Catal A: Chem*** 102: 163-174, 1995.

22. a) RUETTE F. VALENCIA N., SANCHEZ DELGADO R. ***J Am Chem Soc*** 111: 40- 46, 1989.
b) LOBOS S, SIERRAALTA A., RUETTE F., RODRÍGUEZ ARIAS E.N. ***J Mol Catal A: Chem*** 192: 203-216, 2003.

23. GRIFFE B., SIERRAALTA A., RUETTE F., BRITO J.L. ***J Mol Catal*** 168: 265-277, 2001.

24. CLEMENTI E., RAIMONDI D.L. ***J Chem Phys*** 38: 2686-2689, 1963.

25. HARRISON J.F. ***Chem Rev*** 100: 679-716, 2000.

26. a) HUBER K.P., HERZBERG G. ***Constants of Diatomic Molecules.*** Van Nostrand Reinhold, New York, 1979.
b) SOSA R.M., GARDIOL P., BELTRAME G. ***Int J Quant Chem*** 65: 919-928, 1997.
c) DAOUDI A., TOUIMI BENJELLOUN A., FLAMENT J.P., BERTHIER G. ***J Mol Spect*** 194: 8-16, 1999.
d) ***Handbook of Chemistry and Physics***, 79th Ed. CRC press, New York, 1999.
e) ELUSTONDO F., MASCETTI J., PAPAI I. ***J Phys Chem A*** 104: 3572-3578, 2000.
f) CHEN M., ZHOU M., ZHANG L., QIN Q. ***J Phys Chem A*** 104: 8627-8631, 2000.
g) BOLDYREV A., LI X., WANG L. ***J Chem Phys*** 112: 3627-3632, 2000.
h) YANAGISAWA S., TSUNEDA T., HIRAO K. ***J Comp Chem*** 22:1995-2009, 2001.